LBNL–39268

Dense Stellar Matter and Structure of Neutron Stars

Fridolin Weber* and Norman K. Glendenning

Nuclear Science Division and
Institute for Nuclear & Particle Astrophysics
Lawrence Berkeley National Laboratory
University of California
Berkeley, California 94720, USA
Email: fweber@nsdssd.lbl.gov

February 1, 2008

Presented by F. Weber at the
3rd Mario Schönberg School on Physics
João Pessoa, Brazil
July 22 – August 2, 1996
To be published in the Brazilian Journal
of Teaching Physics

*Home institute: Ludwig–Maximilians University of Munich, Institute for Theoretical Physics, Theresienstrasse 37, W-80333 Munich, Germany.

Contents

Dense Stellar Matter and Structure of Neutron Stars

Fridolin Weber and Norman K. Glendenning

Nuclear Science Division and
Institute for Nuclear & Particle Astrophysics
Lawrence Berkeley National Laboratory
University of California
Berkeley, California 94720, USA
Email: fweber@nsdssd.lbl.gov

Abstract

After giving an overview of the history and idea of neutron stars, I shall discuss, in part one of my lectures, the physics of dense neutron star matter. In this connection concepts like chemical equilibrium and electric charge neutrality will be outlined, and the baryonic and mesonic degrees of freedom of neutron star matter as well as the transition of confined hadronic matter into quark matter at supernuclear densities are studied. Special emphasis is put onto the possible absolute stability of strange quark matter. Finally models for the equation of state of dense neutron star matter, which account for various physical possibilities concerning the unknown behavior of superdense neutron star matter, will be derived in the framework of relativistic nuclear field theory. Part two of my lectures deals with the construction of models of static as well as rapidly rotating neutron stars and an investigation of the cooling behavior of such objects. Both is performed in the framework of Einstein's theory of general relativity. For this purpose the broad collection of models for the equation of state, derived in part one, will be used as an input. Finally, in part three a comparison of the theoretically computed neutron star properties (e.g., masses, radii, moments of inertia, red and blueshifts, limiting rotational periods, cooling behavior) with the body of observed data will be performed. From this conclusions about the interior structure of neutron stars – and thus the behavior of matter at extreme densities – will be drawn.

1 Introduction

Neutron stars contain matter in one of the densest forms found in the universe. Matter in their cores possesses densities ranging from a few times ρ_0 to an order of magnitude higher. Here $\rho_0 = 0.15$ nucleons/fm^3 denotes the density of normal nuclear matter, which corresponds to a mass density of 2.5×10^{14} g/cm^3. The number of baryons forming a neutron star is of the order of $A \approx 10^{57}$. The understanding of matter

under such extreme conditions of density is one of the central but also most complex problems of physics.

Neutron stars are associated with two classes of astrophysical objects: Pulsars [1], which are generally accepted to be rotating neutron stars (the fastest so far observed ones have rotational periods of $P = 1.6$ ms, which corresponds to about 620 rotations per second), and compact X-ray sources (e.g., Her X-1 and Vela X-1), certain of which are neutron stars in close binary orbits with an ordinary star. The first millisecond pulsar was discovered in 1982 [2], and in the next seven years about one a year has been found. The situation has changed radically with the recent discovery of an anomalously large population of millisecond pulsars in globular clusters [3], where the density of stars is roughly 1000 times that in the field of the galaxy and which are therefore very favorable environments for the formation of rapidly rotating pulsars that have been spun up by means of mass accretion from a binary companion. At present about 700 pulsars are known, and the discovery rate of new ones is rather high.

As just outlined, neutron stars are objects of highly compressed matter so that the geometry of space-time is changed considerably from flat space. Thus for the construction of realistic models of rapidly rotating compact stars one has to resort to Einstein's theory of general relativity [4, 5, 6, 7, 8, 9]. The equation of state of the stellar matter, i.e., pressure as a function of energy density, is the basic input quantity whose knowledge over a broad range of densities (ranging from the density of iron at the star's surface up to ~ 15 times the density of normal nuclear matter reached in the cores of massive stars) is necessary in order to solve Einstein's equations. Unfortunately the physical behavior of matter under such extreme densities as in the cores of massive stars is rather uncertain and the associated equation of state is only poorly known. The models derived for it differ considerably with respect to the dependence of pressure on density, which has its origin in various sources. To mention several are: (1) the many-body technique used to determine the equation of state, (2) the model for the nucleon-nucleon interaction, (3) description of electrically charge neutral neutron star matter in terms of either (a) only neutrons, (b) neutrons and protons in β equilibrium with electrons and muons, or (c) nucleons, hyperons and more massive baryon states in β equilibrium with leptons, (4) inclusion of pion/kaon condensation, and (5) treatment of the transition of confined hadronic matter into quark matter. It is the purpose of this work to outline the present status of dense matter calculations, explore the compatibility of the properties of non-rotating and rotating compact star models, which are constructed for a collection of equations of state which accounts for items (1)–(5) from above, with observed data, and investigate the properties of hypothetical strange (quark matter) stars [10, 11, 12]. The latter would constitute the true nature of neutron stars if strange quark matter should be more stable than ordinary nucleonic matter.

2 Equation of state of dense neutron star matter

2.1 Theoretical framework

2.1.1 Non-relativistic approach

For non-relativistic models, the starting point is a phenomenological nucleon-nucleon interaction. In the case of the equations of state reported here, different two-nucleon potentials (denoted V_{ij}) which fit nucleon-nucleon scattering data and deuteron properties have been employed. Most of these two-nucleon potentials are supplemented with three-nucleon interactions (denoted V_{ijk}). The hamiltonian is of the form

$$H \;=\; \sum_i \left(\frac{-\hbar^2}{2\,m} \right) \nabla_i^2 \;+\; \sum_{i<j} V_{ij} \;+\; \sum_{i<j<k} V_{ijk} \;. \tag{1}$$

The many-body method adopted to solve the Schroedinger equation is based on the variational approach [13, 14, 15] where a variational trial function $|\Psi_v>$ is constructed from a symmetrized product of two-body correlation operators (F_{ij}) acting on an unperturbed ground-state, i.e.,

$$|\Psi_v> = \left[\hat{S} \prod_{i<j} F_{ij} \right] |\Phi> \,, \tag{2}$$

where $|\Phi>$ denotes the antisymmetrized Fermi-gas wave function,

$$|\Phi> = \hat{A} \prod_j \exp(i\,\boldsymbol{p}_j \cdot \boldsymbol{x}_j) \;. \tag{3}$$

The correlation operator contains variational parameters which are varied to minimize the energy per baryon for a given density ρ (see Refs. [13, 14, 15, 16] for details):

$$E_v(\rho) \;=\; \min \;\; \left\{ \frac{<\,\Psi_v\,|\,H\,|\,\Psi_v\,>}{<\,\Psi_v\,|\,\Psi_v\,>} \right\} \;\;\geq\;\; E_0 \;. \tag{4}$$

As indicated, E_v constitutes an upper bound to the ground-state energy E_0. The energy density $\epsilon(\rho)$ and pressure $P(\rho)$ are obtained from Eq. (4) by

$$\epsilon(\rho) \;=\; \rho\,[E_v(\rho) \,+\, m] \;, \qquad\qquad P(\rho) \;=\; \rho^2\,\frac{\partial}{\partial \rho}\,E_v(\rho) \;, \tag{5}$$

which leads to the equation of state in the form $P(\epsilon)$ used for the star structure calculations here.

2.1.2 Relativistic approach

As discussed elsewhere [9, 17], the lagrangian governing the dynamics of many-baryon (-lepton) neutron-star matter has the following structure:

$$\begin{aligned} \mathcal{L}(x) \;\; &= \sum_{B=p,n,\Sigma^{\pm,0},\Lambda,\Xi^{0,-},\Delta^{++,+,0,-}} \mathcal{L}_B^0(x) \\ &+ \sum_{M=\sigma,\omega,\pi,\varrho,\eta,\delta,\phi} \left\{ \mathcal{L}_M^0(x) \;+ \sum_{B=p,n,\ldots,\Delta^{++,+,0,-}} \mathcal{L}_{B,M}^{\rm Int}(x) \right\} + \sum_{\lambda=e^-,\mu^-} \mathcal{L}_\lambda(x) \;. \end{aligned} \tag{6}$$

Table 1: Masses, electric charges (q_B) and quantum numbers (spin (J_B), isospin (I_B), strangeness (S_B), hypercharge (Y_B), third component of isospin (I_{3B})) of the baryons included in the determination of the equation of state of neutron star matter.

Baryon (B)	m_B [MeV]	J_B	I_B	S_B	Y_B	I_{3B}	q_B
n	939.6	1/2	1/2	0	1	$-1/2$	0
p	938.3	1/2	1/2	0	1	1/2	1
Σ^+	1189	1/2	1	-1	0	1	1
Σ^0	1193	1/2	1	-1	0	0	0
Σ^-	1197	1/2	1	-1	0	-1	-1
Λ	1116	1/2	0	-1	0	0	0
Ξ^0	1315	1/2	1/2	-2	-1	1/2	0
Ξ^-	1321	1/2	1/2	-2	-1	$-1/2$	-1
Δ^{++}	1232	3/2	3/2	0	1	3/2	2
Δ^+	1232	3/2	3/2	0	1	1/2	1
Δ^0	1232	3/2	3/2	0	1	$-1/2$	0
Δ^-	1232	3/2	3/2	0	1	$-3/2$	-1

The subscript B runs over all baryon species that become populated in dense star matter, which are listed in Table 1. The nuclear forces are mediated by that collection of scalar, vector, and isovector mesons (M) that is used for the construction of relativistic one-boson-exchange potentials [18, 19]. The equations of motion resulting from Eq. (6) for the various baryon and meson field operators (given in [9, 17]) are to be solved subject to the conditions of electric charge neutrality, $\rho^{\rm el}_{\rm tot} = \rho^{\rm el}_{\rm Bary} + \rho^{\rm el}_{\rm Lep} \equiv 0$, which leads to

$$\sum_B q_B \, (2J_B+1) \, \frac{p^3_{F,B}}{6\pi^2} \; - \; \Big[\sum_{\lambda=e,\mu} \frac{p^3_{F,\lambda}}{3\pi^2} \; + \; \varrho_\pi \, \Theta(\mu^\pi - m_\pi) \Big] \; = \; 0 \; , \tag{7}$$

and β (chemical) equilibrium [20, 21],

$$\mu^B = \mu^n - q_B \, \mu^e \; , \tag{8}$$

where μ^n and μ^e denote the chemical potentials of neutrons and electrons, whose knowledge is sufficient to find the chemical potential of any other baryon of electric charge q_B present in the system. To solve the equations of chemically equilibrated many baryon matter we apply the Greens function method, which is outlined next.

The starting point is the Martin-Schwinger hierarchy of coupled Greens functions [22, 23]. In the lowest order, the Martin-Schwinger hierarchy can be truncated by factorizing the four-point Greens function $g_2(1,2;1'2')$ [unprimed (primed) arguments refer to ingoing (outgoing) particles] into a product of two-point Greens functions g [$\equiv g_1(1';1')$]. This leads to the well-known relativistic Hartree (i.e., mean-field) and Hartree-Fock approximations. The T-matrix approximation (also known as Λ or ladder approximation), which goes beyond this, truncates the Martin-Schwinger

hierarchy by factorizing the six-point Greens function $g_3(123;1'2'3')$ into products of four- and two-point functions by which dynamical two-particle correlations in matter - which are connected with the two-body potential (denoted v) - are taken into account. The main problem which one encounters hereby is the calculation of the effective scattering matrix (effective two-particle potential) in matter, T, which satisfies

$$T \;=\; v - v^{\rm ex} + \int v\;\Lambda\;T\;. \tag{9}$$

We have restricted ourselves to the so-called Λ^{00} approximation, for which the nucleon-nucleon propagator is given by the product of two free two-point Greens functions, i.e., $\Lambda = \Lambda^{00} \equiv ig^0g^0$, and the relativistic Brueckner-Hartree-Fock (RBHF) approach, where both intermediate baryons feel the nuclear background medium and scatter only into states outside the Fermi sea [24, 25, 26]. The basic input quantity in Eq. (9) is the nucleon-nucleon interaction in free space as derived, for example, in the Bonn meson-exchange model [19]. We have adopted the latest version of this interaction together with Brockmann's potentials A–C to compute the T matrix in neutron matter up to several times nuclear matter density [7, 24, 25, 26]. The important feature of such meson-exchange models is that the potential parameters are adjusted to the two-body nucleon-nucleon scattering data and the properties of the deuteron, whereby (in this sense) a parameter-free treatment of the many-body problem is achieved. The "Born" approximation of T sums the various meson potentials of the nucleon-nucleon interaction in free space, i.e.,

$$< 12 \mid v \mid 1'2' > = \sum_{M=\sigma,\omega,\pi,\rho,\eta,\delta,\phi} \delta^4_{11'}\;\;\Gamma^M_{11'}\;\;\Delta^M_{12}\;\;\Gamma^M_{22'}\;\;\delta^4_{22'}\;, \tag{10}$$

and thus neglects dynamical nucleon-nucleon correlations. It is this approximation which leads to the relativistic Hartree and Hartree-Fock approximations [9, 27, 28, 21]. The symbol Γ^M in Eq. (10) stands for the various meson-nucleon vertices, and Δ^M denotes the free meson propagator of a meson of type M.

The nucleon self-energy (effective one-particle potential) is obtained from the T matrix as [9, 29]

$$\Sigma^B \;=\; i\sum_{B'}\int\;\Big[\;{\rm tr}\;\Big(T^{BB'}\;g^{B'}\Big) - T^{BB'}\;g^{B'}\;\Big]\;, \tag{11}$$

where $B' = p, n, \Sigma^{\pm,0}, \Lambda, \Xi^{0,-}, \Delta^{++,+,0,-}$ sums all the charged baryon states whose threshold densities are reached in the cores of neutron star models. The baryon propagators in Eq. (11) are given as the solutions of Dyson's equation,

$$g^B \;=\; g^{0\,B} \;+\; g^{0\,B}\;\Sigma^B(\{g^{B'}\})\;g^B\;, \tag{12}$$

which terminates the set of equations that are to be solved self-consistently. The diagrammatic representation of the second term in Dyson's equation, $g^{0\,B}\Sigma^B g^B$, is given in Fig. 1. There, single lines denote the free propagator, $g^{0\,B}$, and double lines refer to the self-consistent propagator in matter, g^B. This term corrects the free propagators (first term) for medium effects arising from the Fermi sea of filled baryon

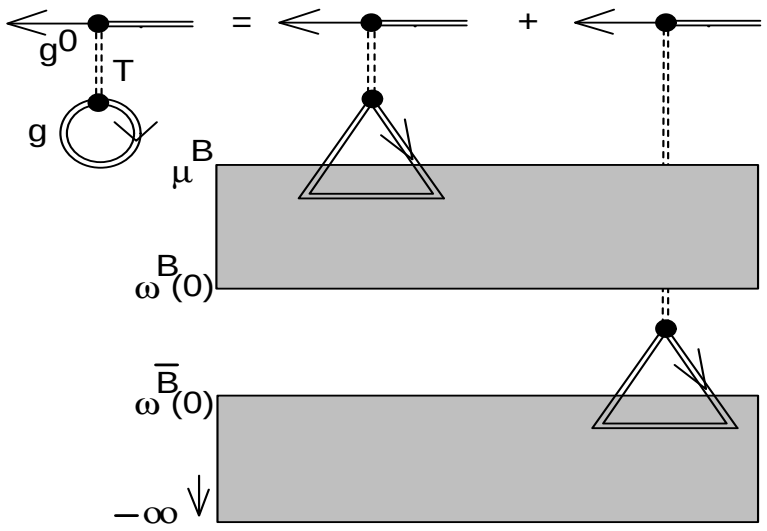

Figure 1: Graphical representation of the self-energy contributions (second term in Eq. (12)) arising from both the Fermi sea, i.e., nuclear matter consisting of filled baryon states of energies $\omega^B(0) \leq \omega^B(p) \leq \mu^B$ (upper graph), as well as Dirac sea (states $-\infty < \omega^{\bar{B}}(p) \leq \omega^{\bar{B}}(0)$, lower graph). The former (latter) lead to so-called medium (vacuum) polarization contributions [30, 31].

states, i.e., the nuclear-matter medium (upper shaded area in Fig. 1), within which the baryons move.[1] Obviously these vanish for baryons propagating in free space, for which $\Sigma^B \equiv 0$. Note that the determination of g^B from Dyson's equation leads to a self-consistent treatment of the coupled matter equations (9)–(12).

The equation of state follows from the stress-energy density tensor, $\mathcal{T}_{\mu\nu}$, of the system as

$$E(\rho) = < \mathcal{T}_{00} > /\rho - m \,, \qquad \text{where} \tag{13}$$

$$\mathcal{T}_{\mu\nu}(x) = \sum_{\chi=B,\lambda} \partial_\nu \Psi_\chi(x) \, \frac{\partial \mathcal{L}(x)}{\partial \left(\partial^\mu \Psi_\chi(x)\right)} - g_{\mu\nu} \, \mathcal{L}(x) \,. \tag{14}$$

The sum in the latter equation sums the contributions coming from the baryons and leptons ($\lambda = e, \mu$). The quantity $\mathcal{L}$ denotes the lagrangian given in Eq. (6) (see Ref. [21] for details). The pressure is obtained from $E(\rho)$ via Eq. (5).

[1] Contributions coming from the lower shaded area account for vacuum polarization corrections. The so-called no-sea approximation, which has been applied for the determination of most of the equations of state presented in Sect. 2.2, neglects such corrections. A critical discussion of the influence of vacuum renormalization on the equation of state of high-density matter has been performed in Ref. [32]. It was found that these have negligible influence on the equation of state up to densities of at least ten times normal nuclear matter density, provided the coupling constants are tightly constrained by the saturation properties of nuclear matter. In the present paper, vacuum polarization contributions are contained in equations of state denoted G_{300} and G^{π}_{300} (see Table 2).

Table 2: Nuclear equations of state applied for the construction of models of general relativistic (rotating) neutron star models.

Label	EOS	Description (see text)	Reference
	Relativistic field theoretical equations of state		
1	G_{300}	H, K=300	[32]
2	HV	H, K=285	[17, 21]
3	G^{DCM2}_{B180}	Q, K=265, $B^{1/4}=180$	[33, 34]
4	G^{DCM2}_{265}	H, K=265	[35]
5	G^{π}_{300}	H, π, K=300	[32]
6	G^{π}_{200}	H, π, K=200	[36]
7	Λ^{00}_{Bonn} + HV	H, K=186	[7]
8	G^{DCM1}_{225}	H, K=225	[35]
9	G^{DCM1}_{B180}	Q, K=225, $B^{1/4}=180$	[33, 34]
10	HFV	H, Δ, K=376	[21]
11	Λ^{RBHF}_{Bro} + HFV	H, Δ, K=264	[24, 25, 26]
	Non-relativistic potential model equations of state		
12	BJ(I)	H, Δ	[37]
13	WFF(UV_{14}+TNI)	NP, K=261	[16]
14	FP(V_{14}+TNI)	N, K=240	[38]
15	WFF(UV_{14}+UVII)	NP, K=202	[16]
16	WFF(AV_{14}+UVII)	NP, K=209	[16]
17	MS94	N, K=234	[39, 40, 41, 42]

2.2 Models for the nuclear equation of state

A representative collection of nuclear equations of state that are determined in the framework of non-relativistic Schroedinger theory and relativistic nuclear field theory is listed in Table 2. A few of them are graphically shown in Fig. 2, where the pressure is plotted as a function of energy density (in units of the density of normal nuclear matter, $\epsilon_0 = 140$ MeV/fm^3). This collection of equations of state has been applied for the construction of models of general relativistic (rotating) compact star models, which will be presented in Sect. 4. The specific properties of these equations of state are described in Table 2, where the following abbreviations are used: N = pure neutron; NP = n, p, leptons; π = pion condensation; H = composed of n, p, hyperons ($\Sigma^{\pm,0}$, Λ, $\Xi^{0,-}$), and leptons; Δ = Δ_{1232}-resonance; Q = quark hybrid composition, i.e., n, p, hyperons in equilibrium with u, d, s-quarks, leptons; K = incompressibility (in MeV); $B^{1/4}$ = bag constant (in MeV). Not all equations of state of our collection account for neutron matter in full β equilibrium (i.e., entries 13–17). These models treat neutron star matter as being composed of only neutrons, or neutrons and protons in equilibrium with leptons, which is however not the ground-state of neutron star matter predicted by theory [17, 37, 43]. As an example of such an equation of state, we exhibit the FP(V_{14}+TNI) model in Fig. 2. The relativistic equations of state account

for all baryon states that become populated in dense star models constructed from them. As representative examples for the relativistic equations of state, we show the HV, HFV, G_{300}, and G^{DCM1}_{B180} models in Fig. 2. A special feature of the latter equation of state is that it also (as G^{DCM2}_{B180}, which is not shown in Fig. 2) accounts for the possible transition of baryon matter to quark matter. One clearly sees in Fig. 2 the softening of the equation of state, i.e., reduction of pressure for a given density, at $\epsilon \gtrsim (2-3)\,\epsilon_0$ which is caused by the onset of baryon population and/or the transition of baryon matter to quark matter. The stiffer behavior of HFV in comparison with HV at high densities has its origin in the exchange (Fock) contribution that is contained in the former equation of state. An inherent feature of the relativistic equations of state is that they do not violate causality, i.e., the velocity of sound, given by $v_s = c\sqrt{dP/d\epsilon}$, is smaller than the velocity of light (c) at all densities, which is not the case for the non-relativistic models for the equation of state (cf. Table 3). Among the latter only the WFF(UV_{14} + TNI) equation of state does not violate causality up to densities relevant for the construction of models of neutron stars from it.

The nuclear matter properties at saturation density related to our collection of equations of state are summarized in Table 3. The listed quantities are: binding energy of normal nuclear matter at saturation density, E/A; compression modulus, K; effective nucleon mass, M^* ($\equiv m^*/m$, where m denotes the nucleon mass); asymmetry energy, $a_{\rm sy}$. With the exception of $\Lambda^{00}_{\rm Bonn}$ + HV and $\Lambda^{\rm RBHF}_{\rm Bro}$ + HFV, the coupling constants of the relativistic equations of state are determined such that these saturate infinite nuclear matter at densities in the range 0.15 to 0.16 fm^{-3} for a binding energy per nucleon of about -16 MeV. For the $\Lambda^{00}_{\rm Bonn}$ + HV and $\Lambda^{\rm RBHF}_{\rm Bro}$ + HFV equations of state the saturation properties are determined by respectively the relativistic Bonn and Brockmann meson-exchange models for the nucleon-nucleon interaction whose parameters are determined by the free nucleon-nucleon scattering problem and the properties of the deuteron (parameter-free treatment). The influence of dynamical two-particle correlations calculated from the scattering matrix leads for these two equations of state to a relatively soft behavior in the vicinity of the saturation density. This is indicated by the rather small compression moduli K related to these equations of state. All non-relativistic equations of state of our collection, which are determined in the framework of the variational method outlined in Sect. 2.1.1, contain the impact of dynamical two-particle correlations in matter, too. The correlations are calculated for different hamiltonians. With the exception of BJ(I) and MS94, the calculations are performed for the Urbana and Argonne two-nucleon potentials V_{14}, UV_{14} [44] and AV_{14} [45], respectively, supplemented by different models for the three-nucleon interaction. These are the density-dependent three-nucleon interaction of Lagaris and Pandharipande, TNI [46], and the Urbana three-nucleon model, UVII [44]. One sees that nuclear matter is underbound by ≈ 4 MeV for two of these equations of state. The corresponding saturation densities are in the range of 0.17 to 0.19 fm^{-3}, thus nuclear matter saturates at somewhat too large densities for these equations of state. (The empirical saturation density is ≈ 0.15 fm^{-3} [47].) Equations of state labeled 13 and 14 lead to binding energies and saturation densities that are in good agreement with the empirical values which has its origin in the density-dependent

Table 3: Nuclear matter properties of the equations of state used in this work.

Label	EOS	E/A [MeV]	ρ_0 [fm^{-3}]	K [MeV]	M^* [MeV]	$a_{\rm sy}$ [MeV]	ϵ/ϵ_0 †
1	G_{300}	−16.3	0.153	300	0.78	32.5	–
2	HV	−15.98	0.145	285	0.77	36.8	–
3	$\mathrm{G}^{\rm DCM2}_{\rm B180}$	−16.0	0.16	265	0.796	32.5	–
4	$\mathrm{G}^{\rm DCM2}_{265}$	−16.0	0.16	265	0.796	32.5	–
5	G^{π}_{300}	−16.3	0.153	300	0.78	32.5	–
6	G^{π}_{200}	−15.95	0.145	200	0.8	36.8	–
7	$\Lambda^{00}_{\rm Bonn}+\mathrm{HV}$	−11.9	0.134	186	0.79		–
8	$\mathrm{G}^{\rm DCM1}_{225}$	−16.0	0.16	225	0.796	32.5	–
9	$\mathrm{G}^{\rm DCM1}_{\rm B180}$	−16.0	0.16	225	0.796	32.5	–
10	HFV	−15.54	0.159	376	0.62	30	–
11	$\Lambda^{\rm RBHF}_{\rm Bro}+\mathrm{HFV}$	−14.81	0.170	264	0.66	32	–
12	BJ(I)						23.1
13	WFF(UV_{14}+TNI)	−16.6	0.157	261	0.65	30.8	14
14	FP(V_{14}+TNI)	−16.00	0.159	240	0.64		5.6
15	WFF(UV_{14}+UVII)	−11.5	0.175	202	0.79	29.3	6.5
16	WFF(AV_{14}+UVII)	−12.4	0.194	209	0.66	27.6	7.2
17	MS94	−16.04	0.161	234		32.0	13

† Energy density in units of normal nuclear matter density beyond which the velocity of sound in neutron matter becomes larger (superluminal) than the velocity of light. The symbol "–" indicates that causality is not violated.

three-nucleon interaction TNI.[2] Interesting is the shift of the saturation density obtained for $\Lambda^{00}_{\rm Bonn}+\mathrm{HV}$ and $\Lambda^{\rm RBHF}_{\rm Bro}+\mathrm{HFV}$ – relative to non-relativistic treatments that account for dynamical correlations too – toward smaller densities which is caused by relativity [27, 30, 55, 56, 57].

The four equations of state $\mathrm{G}^{\rm DCM1}_{225}$, $\mathrm{G}^{\rm DCM2}_{265}$, $\mathrm{G}^{\rm DCM1}_{\rm B180}$, and $\mathrm{G}^{\rm DCM2}_{\rm B180}$, which are based on the relativistic lagrangian of Zimanyi and Moszkowski, have only recently been determined [34, 58]. The transition of confined hadronic matter into quark matter is taken into account in equations of state $\mathrm{G}^{\rm DCM1}_{\rm B180}$ (Fig. 2) and $\mathrm{G}^{\rm DCM2}_{\rm B180}$. Here a bag constant of $B^{1/4}=180$ MeV has been used for the determination of the transition of baryon matter into quark matter, which places the energy per baryon of strange matter at 1100 MeV, well above the energy per nucleon in ^{56}Fe ($\approx$ 930 MeV). Most

[2]It is well known that two-particle correlations alone fail in reproducing the empirical values of binding energy and saturation density. In this case the saturation points calculated from the standard Brueckner-Hartree-Fock [13, 48, 49] and non-relativistic T matrix approximations [50, 51, 52] for different nucleon-nucleon interactions fall in a narrow band, often called the Coester band. It appears likely that this band would contain the calculated saturation point for any realistic nucleon-nucleon interaction [53, 54].

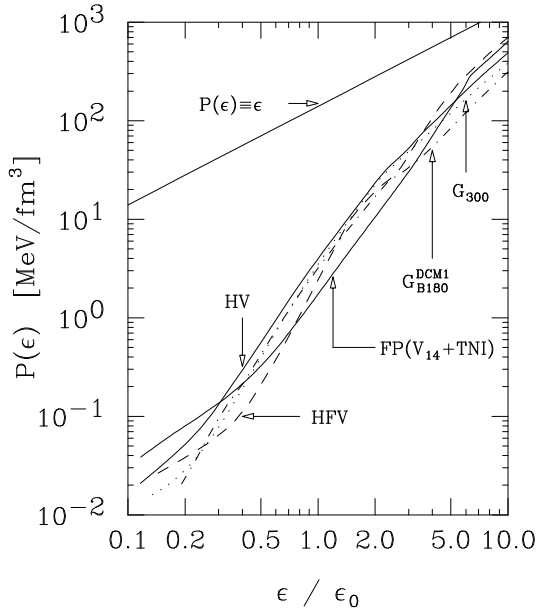

Figure 2: Graphical illustration of the equations of state HV, HFV, FP(V_{14} + TNI), G_{300}, and G^{DCM1}_{B180}.

interestingly, the transition to quark matter sets in already at a density $\epsilon = 2.3\,\epsilon_0$ [33, 34], which lowers the pressure relative to confined hadronic matter. The mixed phase of baryons and quarks ends, i.e. the pure quark phase begins, at $\epsilon \approx 15\,\epsilon_0$, which is larger than the central density encountered in the maximum-mass star model constructed from this equation of state. We stress that these density thresholds are rather different from those computed by other authors in earlier investigations. The reason for this lies in the realization that the transition between confined hadronic matter and quark matter takes place subject to the conservation of baryon and electric charge. Correspondingly, there are two chemical potentials, and the transition of baryon matter to quark matter is to be determined in three-space spanned by pressure and the chemical potentials of the electrons and neutrons. The only existing investigation which accounts for this properly has been performed by Glendenning [33, 34]. Further important differences between the determination of G^{DCM1}_{B180} and earlier (and thus inconsistent) treatments concern the description of the dense interior of compact stars[3] and the approximation of the mixed phase as two components which are separately charge neutral.

[3]If the dense core may be converted to quark matter [59, 60, 61], it must be strange quark matter, since 3-flavor quark matter has a lower energy per baryon than 2-flavor. And just as is the case for the hyperon content of neutron stars, strangeness is not conserved on macroscopic time scales. Many of the earlier discussions [59, 60, 61, 62, 63, 64, 65, 66, 67] have treated the neutron star as pure in neutrons, and the quark phase as consisting of the equivalent number of u and d quarks. However neither is pure neutron matter the ground state of a star nor is a mixture of $n_d = 2\,n_u$! In fact it is a highly excited state, and will quickly weak decay to an approximate equal mixture of u, d, s quarks.

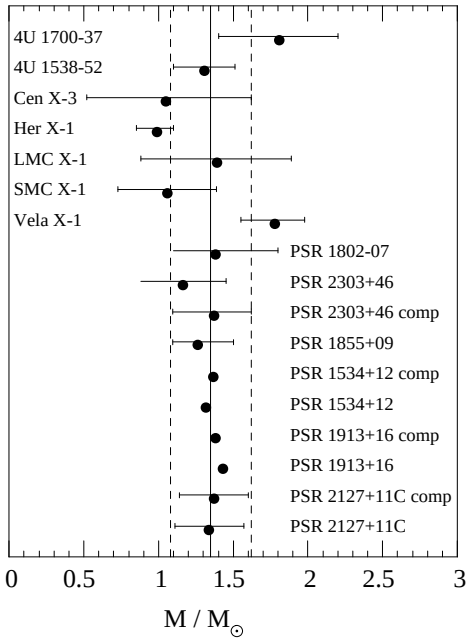

Figure 3: Distribution of observed neutron star masses [70].

3 Observed neutron star properties

The global neutron star properties such as masses, rotational frequencies, radii, moments of inertia, redshifts, etc. are known to be sensitive to the adopted microscopic model for the nucleon-nucleon interaction or, in other words, to the nuclear equation of state [68]. Thus, by means of comparing the theoretically determined values for these quantities with observed ones one may hope to learn about the physical behavior of matter at super-nuclear densities. In the following we briefly summarize important star properties.

3.1 Masses

The gravitational mass is of special importance since it can be inferred directly from observations of X-ray binaries and binary pulsars (e.g., the Hulse-Taylor radio pulsar PSR 1913+16 [69]). Rappaport and Joss were the first who deduced neutron star masses for six X-ray binaries [71]. A reexamination of these masses became possible owing to the improved determinations of orbital parameters [72]. Improved values are shown in Fig. 3. The objects 3U1700–37 and Cyg X–1 are two non-pulsating X-ray binaries. It is expected that at least one of these objects, likely Cyg X-1, is a black hole. Very remarkable is the extremely accurately determined mass of the

Hulse-Taylor binary pulsar, PSR 1913+16, which is given by 1.444 ± 0.003 [69].

In summary, Fig. 3 suggests that the most probable value of neutron star masses, as derived from observations of binary X-ray pulsars, is close to about $1.4\,M_\odot$, and that the masses of individual neutron stars are likely to be in the range $1.1 \lesssim M/M_\odot \lesssim 1.8$ [72].

3.2 Rotational frequencies of fast pulsars

The rotational periods of fast pulsars provide conditions on the equation of state when combined with the mass constraint [73]. As already mentioned in Sect. 1, the fastest so far observed pulsars have rotational periods of 1.6 ms (i.e., 620 Hz). The successful model for the nuclear equation of state, therefore, must account for rotational neutron star periods of at least $P = 1.6$ ms as well as masses that lie in range listed in Sect. 3.1.

3.3 Radii

Direct radius determinations for neutron stars do not exist. However, combinations of data of 10 well-observed X-ray bursters with special theoretical assumptions lead Van Paradijs [74] to the conclusion that the emitting surface has a radius of about 8.5 km. This value, as pointed out in [75], may be underestimated by a factor of two. Fujimoto and Taam [76] derived from the observational data of the X-ray burst source MXB 1636–536, under rather uncertain theoretical assumptions, a neutron star mass and radius of $1.45\,M_\odot$ and 10.3 km. An error analysis lead them to predicting mass and radius ranges of 1.28 to $1.65\,M_\odot$ and 9.1 to 11.3 km, respectively. When comparing these values with computed neutron star data, however, one should be aware of the fact that burster are suspected, but not known, to be neutron stars.

3.4 Moment of inertia

Another global neutron star property is the moment of inertia, I. Early estimates of the energy-loss rate from pulsars [77] spanned a wide range of I, i.e., $7 \times 10^{43} < I < 7 \times 10^{44}$ g/cm^3. From the luminosity of the Crab nebula ($\sim 2 - 4 \times 10^{38}$ erg/sec), several authors have found a lower bound on the moment of inertia of the pulsar given by $I \gtrsim 4 - 8 \times 10^{44}$ g cm^2 [78, 79, 80].

3.5 Redshift

Finally we mention the neutron star redshift, z. Liang [81] has considered the neutron star redshift data base provided by measurements of γ-ray burst redshifted annihilation lines in the range $300 - 511$ keV. These bursts have widely been interpreted as gravitationally redshifted 511 keV $e^\pm$ pair annihilation lines from the surfaces of neutron stars. From this he showed that there is tentative evidence (if the interpretation is correct) to support a neutron star redshift range of $0.2 \leq z \leq 0.5$, with the highest concentration in the narrower range $0.25 \leq z \leq 0.35$. A particular role plays

the source of the 1979 March 5 γ-ray burst source, which has been identified with SNR N49 by its position. From the interpretation of its emission, which has a peak at ~ 430 keV, as the 511 keV $e^{\pm}$ annihilation line [82, 83] the resulting gravitational redshift has a value of $z = 0.23 \pm 0.05$.

4 Properties of neutron star models

4.1 Non-rotating star models

The structure of spherical neutron stars is determined by the Oppenheimer-Volkoff equations [84, 85],

$$\frac{dP}{dr} = -\frac{\epsilon(r)\, m(r)\, [1 + P(r)/\epsilon(r)]\, [1 + 4\pi r^3 P(r)/m(r)]}{r^2\, [1 - 2m(r)/r]}\,, \tag{15}$$

which describe a compact stellar configuration in hydrostatic equilibrium. (Here we use units for which the gravitational constant and velocity of light are $G = c = 1$. Hence $M_\odot = 1.5$ km.) The boundary condition reads $P(r = 0) \equiv P_c = P(\epsilon_c)$, where ϵ_c denotes the energy density at the star's center, which constitutes the free parameter that is to be specified when solving the above differential equation for a given equation of state. The latter determines P_c and the energy density for all pressure values $P < P_c$. The pressure is to be computed out to that radial distance where $P(r) = 0$, which determines the star's radius R, i.e., $P(r = R) = 0$. The mass contained in a sphere of radius r ($\leq R$), denoted by $m(r)$, follows from $\epsilon(r)$ as

$$m(r) = 4\pi \int_0^r dr'\, r'^2\, \epsilon(r')\,. \tag{16}$$

The star's total (gravitational) mass is given by $M \equiv m(R)$.

Figure 4 exhibits the gravitational mass of non-rotating neutron stars as a function of central energy density for a sample of equations of state of Table 2. Each star sequence is shown up to densities that are slightly larger than those of the maximum-mass star (indicated by tick marks) of each sequence. Stars beyond the mass peak are unstable against radial oscillations and thus cannot exist stably (collapse to black holes) in nature. One sees that all equations of state are able to support non-rotating neutron star models of gravitational masses $M \geq M(\mathrm{PSR}\ 1913 + 16)$. On the other hand, rather massive stars of say $M \gtrsim 2\, M_\odot$ can only be obtained for those models of the equation of state that exhibit a rather stiff behavior at super nuclear densities (cf. Fig. 2). The largest maximum-mass value, $M = 2.2\, M_\odot$, is obtained for HFV, which is caused by the exchange term contained in that model. Knowledge of the maximum-mass value is of great importance for two reasons. Firstly, quite a few neutron star masses are known (Sect. 3), and the largest of these imposes a lower bound on the maximum-mass of a theoretical model. The current lower bound is about $1.56\, M_\odot$ [neutron star 4U 0900–40 ($\equiv$ Vela X–1)], which, as we have just seen, does not set a too stringent constraint on the nuclear equation of state. The situation

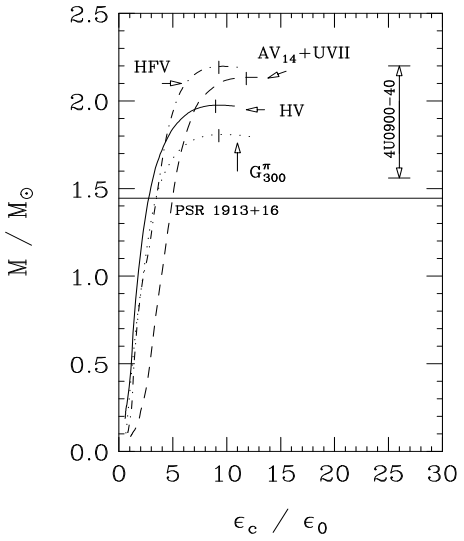

Figure 4: Non-rotating neutron star mass as a function of central density.

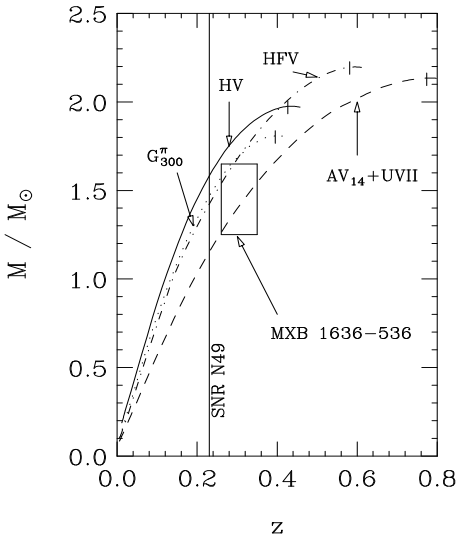

Figure 5: Non-rotating neutron star mass as a function of redshift.

could easily change if an accurate future determination of the mass of neutron star 4U 0900–40 (see Fig. 4) should result in a value that is close to its present upper bound of $1.98\,M_\odot$. In this case most of the equations of state of our collection would be ruled out. The second reason is that the maximum mass can be useful in identifying black hole candidates [86, 87, 88]. For example, if the mass of a compact companion of an optical star is determined to exceed the maximum mass of a neutron star it must be a black hole. Since the maximum mass of stable neutron stars in our theory is $2.2\,M_\odot$, compact companions being more massive than that value are predicted to be black holes.

The neutron star mass as a function of gravitational redshift, defined as

$$z = \frac{1}{\sqrt{1-2M/R}} - 1 \,, \tag{17}$$

is shown in Fig. 5 for the same sample of equations of state as in Fig. 4. One sees that the maximum-mass stars have redshifts in the range $0.4 \lesssim z \lesssim 0.8$, depending on the softness (stiffness) of the equation of state. Neutron stars of typically $M \approx 1.5\,M_\odot$ (e.g., PSR 1913+16) are predicted to have redshifts in the considerably narrower range $0.2 \leq z \leq 0.32$. The solid rectangle covers masses and redshifts in the ranges of $1.30 \leq M/M_\odot \leq 1.65$ and $0.25 \leq z \leq 0.35$, respectively. As outlined in Sects. 3.3 and 3.5, the former range has been determined from observational data of X-ray burst source MXB 1636–536 [76], while the latter is based on the neutron star redshift data base provided by measurements of gamma-ray burst pair annihilation lines [81]. (Note the remarks in Sects. 3.3 and 3.5 concerning the interpretation of these data.) From the redshift value of SNR N49 (if correct) we predict a neutron mass star of $1.1 \lesssim M/M_\odot \lesssim 1.6$, which is consistent with the observed mass range given in Sect.

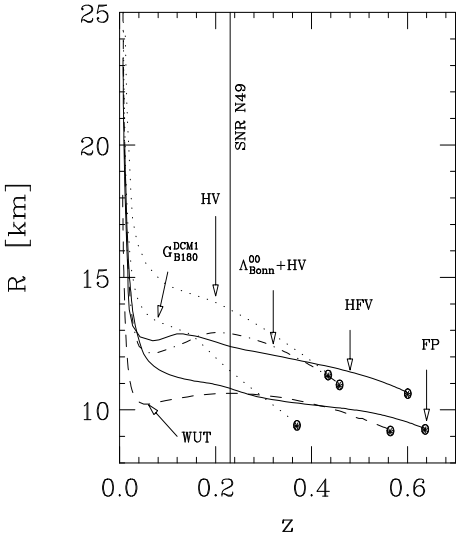

Figure 6: Radius as a function of redshift for a sample of equations of state of Table 2.

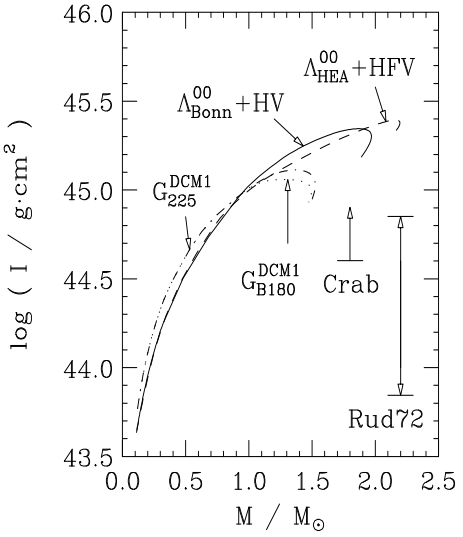

Figure 7: Moment of inertia as a function of mass for a sample of equations of state of Table 2.

3.1. The relativistic equations of state set a narrower mass limit for SNR N49 given by $1.4 \lesssim M/M_\odot \lesssim 1.6$.

Figure 6 displays the radius as a function of gravitational redshift. The solid dots refer to the maximum-mass star of each sequence. Of course, stars at their termination points possess the largest redshifts, and these become the smaller the lighter the stars. Under the assumption that the annihilation line interpretation is correct (Sect. 3.5), SNR N49 is predicted to have a radius in the range of 10 to 14 km. The relativistic equations of state lead to a narrower radii range, i.e., 12.5 to 14 km. In general, the non-relativistic equations of state lead to smaller radii for a given redshift. The reason for this lies in the relatively soft (stiff) behavior at low (high) nuclear densities of the non-relativistic equations of state, which is less pronounced for the relativistic Hartree and Hartree-Fock equations of state. (The softness/stiffness of the relativistic Brueckner-Hartree-Fock equation of state, however, is qualitatively similar to the one obtained for the non-relativistic models.) Small radius values of star models are important in order to achieve rapid rotation. For that reason star models constructed for the non-relativistic equations of state possess limiting rotational periods that are smaller than those obtained for the relativistic equations of state, as will be discussed in Sect. 4.2). However, because of causality violation of the non-relativistic equations of state at high nuclear densities (Sect. 2.2), this trend may be an artifact.

In Fig. 7 we show the moment of inertia of neutron stars, given by [89]

$$I(\Omega) = 4\,\pi \int_0^{\pi/2} d\theta \int_0^{R(\theta)} dr\, e^{\lambda+\mu+\nu+\psi}\, \frac{\epsilon + P(\epsilon)}{e^{2\nu-2\psi} - (\Omega-\omega)^2}\, \frac{\Omega-\omega}{\Omega}\ , \qquad (18)$$

as a function of gravitational mass. In Sect. 2.2 we have pointed out that, in general, the inclusion of baryon population in neutron star matter as well as the possible transition of confined hadronic matter to quark matter causes a softening of the equation of state, which leads to somewhat smaller star masses and radii. From the functional dependence of I on radius and mass, which is of the form $I \propto R^2\, M$, one expects a relative decrease of the moment of inertia of star models constructed for such equation of state. Of course, the general relativistic expression for the moment of inertia, given in Eq. (18), is much more complicated. It accounts for the dragging effect of the local inertial frames (frequency dependence $\omega(r,\theta)$) and the curvature of space-time [89]. Nevertheless the qualitative dependence of I on mass and radius as expressed in the classical expression remains valid [68]. Estimates for the upper and lower bounds on the moment of inertia of the Crab pulsar derived from the pulsar's energy loss rate (labeled Rud72), and the lower bound on the moment of inertia derived from the luminosity of the Crab nebula (labeled Crab) [78, 79, 80] are shown in Fig. 7 for the purpose of comparison. (The arrows refer only to the value of $I_{\rm Crab}$ and not to its mass, which is not known.)

4.2 Rotating star models

4.2.1 Minimal rotational periods

Figures 8 and 9 exhibit the limiting rotational periods of compact stars, which is set by the gravitational radiation reaction-driven instability [90, 91, 92]. It originates from counter-rotating surface vibrational modes, which at sufficiently high rotational star frequencies are dragged forward. In this case, gravitational radiation which inevitably accompanies the aspherical transport of matter does not damp the modes, but rather drives them [93, 94]. Viscosity plays the important role of damping such gravitational-wave radiation-reaction instabilities at a sufficiently reduced rotational frequency such that the viscous damping rate and power in gravity waves are comparable [95]. The instability modes are taken to have the dependence $\exp[i\omega_m(\Omega)t + im\phi - t/\tau_m(\Omega)]$, where ω_m is the frequency of the surface mode which depends on the angular velocity Ω of the star, ϕ denotes the azimuthal angle, and τ_m is the time scale for the mode which determines its growth or damping. The rotation frequency Ω at which it changes sign is the critical frequency for the particular mode, m (=2,3,4,...). It is conveniently expressed as the frequency, denoted by Ω_m^ν, that solves [90] (ν refers to the viscosity dependence, see below)

$$\Omega_m^\nu \;=\; \frac{\omega_m(0)}{m}\,\left[\tilde{\alpha}_m(\Omega_m^\nu) + \tilde{\gamma}_m(\Omega_m^\nu)\left(\frac{\tau_{g,m}}{\tau_{\nu,m}}\right)^{\frac{1}{2\,m+1}}\right]\,, \tag{19}$$

where

$$\omega_m(0) \;\equiv\; \sqrt{\frac{2\,m\,(m-1)}{2\,m\,+\,1}\,\frac{M}{R^3}} \tag{20}$$

is the frequency of the vibrational mode in a non-rotating star. The time scales for gravitational radiation-reaction [96], $\tau_{g,m}$, and for viscous damping time [97], $\tau_{\nu,m}$, are

given by

$$\tau_{g,m} = \frac{2}{3}\,\frac{(m-1)\,[(2m+1)!!]^2}{(m+1)\,(m+2)}\,\left(\frac{2m+1}{2m(m-1)}\right)^m\,\left(\frac{R}{M}\right)^{m+1}\,R\,, \tag{21}$$

$$\tau_{\nu,m} = \frac{R^2}{(2m+1)\,(m-1)}\,\frac{1}{\nu}\,, \tag{22}$$

respectively. The shear viscosity is denoted by ν. It depends on the temperature, T, of the star [$\nu(T) \propto T^{-2}$]. It is small in very hot ($T \approx 10^{10}$ K) and therefore young stars and larger in cold ones. A characteristic feature of equations (19)–(22) is that Ω_m^ν merely depends on radius and mass (R and M) of the spherical star model, which eases solving these equations considerably.

The functions $\tilde{\alpha}_m$ and $\tilde{\gamma}_m$ contain information about the pulsation of the rotating star models and are difficult to determine [90, 98]. A reasonable first step is to replace them by their corresponding Maclaurin spheroid functions α_m and γ_m [90, 98]. We therefore take $\alpha_m(\Omega_m)$ and $\gamma_m(\Omega_m)$ as calculated in Refs. [99, 100] for the oscillations of rapidly rotating inhomogeneous Newtonian stellar models (polytropic index n=1), and Ref. [90] for uniform-density Maclaurin spheroids (i.e., n=0), respectively. Managan has shown that Ω_m^ν depends much more strongly on the equation of state and the mass of the neutron star model [through $\omega_m(0)$ and $\tau_{g,m}$, see Eqs. (20] and (21)) than on the polytropic index assumed in calculating α_m [101].

Figure 8 shows the critical rotational periods, at which emission of gravity waves sets in in hot ($T = 10^{10}$ K) pulsars, newly born in supernova explosions. Figure 9 is the analog of Fig. 8, but for old and therefore cold compact stars of temperature $T = 10^6$ K, like neutron stars in binary systems that are being spun up (and thereby reheated) by mass accretion from a companion. One sees that the limiting rotational periods P^T ($\equiv 2\pi/\Omega_m^\nu$) are the smaller the more massive (and thus the smaller the radius) the star model (cf. Fig. 6). A comparison between Figs. 8 and 9 shows that the instability periods are shifted toward smaller values the colder the star, due to the larger viscosity in such objects. Consequently, the instability modes of compact stars in binary systems are excited at smaller rotational periods than is the case for hot and newly born pulsars in supernovae.[4] The dependence of P^T on the equation of state is shown too in these figures. One sees that the lower limits on P^T are set by the non-relativistic equation of state labeled 16 due to the small radii values obtained for the star models constructed from it. The relativistic models for the equation of state generally lead to larger rotational periods due to the somewhat larger radii of the associated star models.

The rectangles in Figs. 8 and 9 denoted "observed" cover both the range of observed neutron star masses, $1.1 \lesssim M/M_\odot \lesssim 1.8$ as well as observed pulsar periods,

[4]Sawyer [102] has found that the bulk viscosity of neutron star matter goes as the sixth power of the temperature, as compared with a T^{-2} dependence for the shear viscosity which is treated here. This means that at $T \gtrsim 10^9$ K the bulk viscosity would dominate over the shear viscosity and thus damp the gravitational-wave instability. In this case the instability periods would be shifted toward values that are relatively close to the Kepler period $P_{\rm K}$ [100, 103], which will be discussed below. The latter sets an absolute limit on stable rotation because of mass shedding. Bounds on $P_{\rm K}$ are given in Table 4.

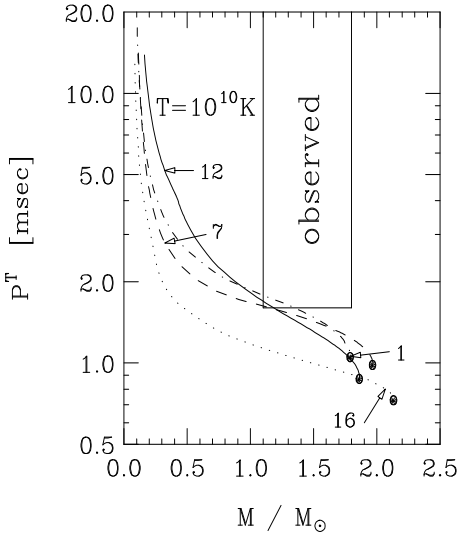

Figure 8: Gravitational radiation-reaction instability period P^T versus mass for newly born stars of temperature $T = 10^{10}$ K [104].

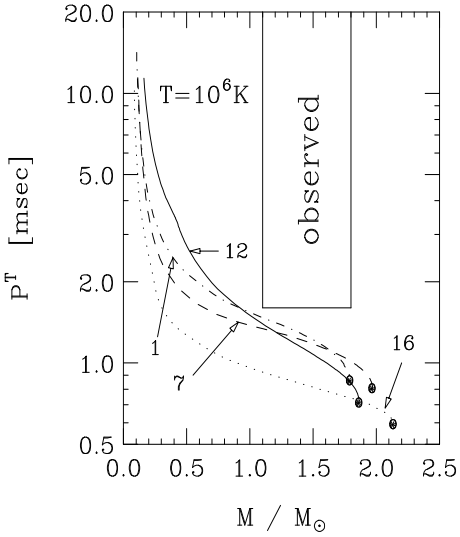

Figure 9: Gravitational radiation-reaction instability period P^T versus mass for old stars of temperature $T = 10^6$ K [104].

i.e., $P \geq 1.6$ ms. One sees that even the most rapidly rotating pulsars so far observed have rotational periods larger that those at which gravity-wave emission sets in and thus can be understood as rotating neutron or hybrid stars.[5] The observation of pulsars possessing masses in the observed range but rotational periods that are smaller than say ~ 1 ms (depending on temperature and thus on the pulsar's history) would be in clear contradiction to our equations of state. Consequently the possible future observation of such pulsars cannot be reconciled – in the framework of our collection of models for superdense neutron star matter – with the interpretation of such objects as rapidly rotating neutron or hybrid stars. This conclusion is strengthened by the construction of neutron star models that are rotating at their Kepler periods, $P_{\rm K}$, at which mass shedding at the star's equator sets in. Therefore this period sets an absolute limit on rapid rotation, which cannot be overcome by any rapidly rotating star. On the basis of neutron star models constructed from the selection of equations of state studied here, the smallest Kepler periods are found to be in the range of $0.7 \lesssim P_{\rm K} \lesssim 1$ ms, depending on the softness of the equation of state[6] (cf. Table 4).

[5]Depending on their composition, compact star models are denoted as neutron, hybrid, or strange stars. Neutron stars consist of protons, neutrons and more massive baryons in β equilibrium with leptons; hybrid stars are compact stars which, in addition to baryons, also contain quarks in their dense cores; hypothetical strange stars consist of (3-flavor) strange quark matter which, by hypothesis, may form the absolute ground-state of strongly interacting matter (see Sect. 5 for more details).

[6]An investigation of this period for neutron stars and other compact objects that is performed without taking recourse to any particular models of dense matter (but derives the limit only on the general principles that: Einstein's equations describe stellar structure, matter is microscopically

$P_{\rm K}$ is given by [4, 9, 106]

$$P_{\rm K} \equiv \frac{2\,\pi}{\Omega_{\rm K}}\,, \text{ with } \Omega_{\rm K} = \omega + \frac{\omega'}{2\psi'} + e^{\nu-\psi}\sqrt{\frac{\nu'}{\psi'} + \Big(\frac{\omega'}{2\psi'}e^{\psi-\nu}\Big)^2}\,. \tag{23}$$

Note that $P_{\rm K}$ can only be obtained by means of solving Eq. (23) self-consistently in combination with Einstein's equation,

$$\mathcal{R}^{\kappa\lambda} \;-\; \frac{1}{2}\,g^{\kappa\lambda}\,\mathcal{R} \;=\; 8\,\pi\,\mathcal{T}^{\kappa\lambda}(\epsilon, P(\epsilon)) \;\;, \tag{24}$$

and the equation of energy-momentum conservation, $\mathcal{T}^{\kappa\lambda}{}_{;\lambda} = 0$, which renders the problem extremely complicated. The quantities $\mathcal{R}^{\kappa\lambda}$, $g^{\kappa\lambda}$, and $\mathcal{R}$ denote the Ricci tensor, metric tensor, and Ricci scalar (scalar curvature), respectively. The dependence of the energy-momentum tensor $\mathcal{T}^{\kappa\lambda}$ on pressure and energy density, P and ϵ respectively, is indicated in Eq. (24). The quantities ω, ν, and ψ in Eq. (23) denote the frame dragging frequency of local inertial frames, and time- and space-like metric functions, respectively.

4.2.2 Bounds on properties of rapidly rotating pulsars

We restrict ourselves to the properties of a rapidly rotating pulsar model having a mass of $M \approx 1.45\,M_\odot$, as supported by the evolutionary history of supermassive stars [75]. The bounds on its properties, whose knowledge is of great importance for the interpretation of fast pulsar, are summarized in Table 4. The listed properties are: period at which the gravitational radiation-reaction instability sets in, P^T (in ms) with star temperature listed in parentheses; Kepler period, $P_{\rm K}$ (in ms); central energy density, ϵ_c (in units of the density of normal nuclear matter); moment of inertia, I (in g cm^2); redshifts of photons emitted at the star's equator in backward ($z_{\rm B}$) and forward ($z_{\rm F}$) direction, defined by

$$z_{\rm B\,/\,F}(\Omega) = e^{-\nu(\Omega)}\;\Big(1 \pm \omega(\Omega)\,e^{\psi(\Omega)-\nu(\Omega)}\Big)^{-1}\;\left(\frac{1 \pm V(\Omega)}{1 \mp V(\Omega)}\right)^{1/2} \;-\; 1\,, \tag{25}$$

and the redshift of photons emitted from the star's pole,

$$z_{\rm p}(\Omega) \quad = \quad e^{-\,\nu(\Omega)} \quad - \quad 1\,. \tag{26}$$

(V denotes the star's velocity at the equator [4, 9]. All other quantities are as in Sect. 4.2.1.) According to Table 4, newly born pulsars observed in supernova explosions can only rotate stably at periods $\gtrsim 1$ ms. Half-millisecond periods, for example, are completely excluded for pulsars made of baryon matter. Therefore, the possible future discovery of a single sub-millisecond pulsar, rotating with a period of say ~ 0.5 ms,

stable, and causality is not violated) has only recently been performed by Glendenning [105]. He establishes a lower bound for the minimum Kepler period for a $M = 1.442\,M_\odot$ neutron star of $P_{\rm K} = 0.33$ ms. Of course the equation of state that nature has chosen need not be the one that allows stars to rotate most rapidly.

Table 4: Lower and upper bounds on the properties of pulsars with $M \approx 1.45\,M_\odot$, calculated for the broad collection of equations of state of Table 2 [108].

	$P^T\,(10^6$ K)	$P^T\,(10^{10}$ K)	$P_{\rm K}$	ϵ_c/ϵ_0	log I	$z_{\rm B}$	$z_{\rm F}$	$z_{\rm p}$
upper bound	1.1	1.5	1	5	45.19	1.05	−0.18	0.45
lower bound	0.8	1.1	0.7	2	44.95	0.59	−0.21	0.23

would give a strong hint that such an object is a rotating strange star, not a neutron star, and that 3-flavor strange quark matter may be the true ground-state of the strong interaction, as pointed out by Glendenning [107]. Old pulsar of $T = 10^6$ K (and mass $M \approx 1.45\,M_\odot$) cannot be spun up to stable rotational periods smaller than ≈ 0.8 ms. Again, the two fastest yet observed pulsars, rotating at 1.6 ms, are compatible with the periods in Table 4, provided their masses are larger than 1 $M_\odot$ [104]. For the purpose of comparison the Kepler period, below which mass shedding at the star's equator sets in, is listed too. It may play a role in cold (hot) pulsar whose rotation is stabilized by its large shear (bulk) viscosity value (see footnote 4 on Sawyers calculation of the viscosity in dense nuclear matter).

5 Strange quark matter stars

5.1 The strange matter hypothesis

The hypothesis that strange quark matter may be the absolute ground state of the strong interaction (not ^{56}Fe) has been raised by Bodmer [109], Witten [10], and Terazawa [110]. If the hypothesis is true, then a separate class of compact stars could exist, which are called strange stars. They form a distinct and disconnected branch of compact stars and are not part of the continuum of equilibrium configurations that include white dwarfs and neutron stars. In principle both strange and neutron stars could exist. However if strange stars exist, the galaxy is likely to be contaminated by strange quark nuggets which would convert all neutron stars to strange stars [107, 111, 112]. This in turn means that the objects known to astronomers as pulsars are probably rotating strange matter stars, not neutron matter stars as is usually assumed. Unfortunately the bulk properties of models of neutron and strange stars of masses that are typical for neutron stars, $1.1 \lesssim M/M_\odot \lesssim 1.8$, are relatively similar and therefore do not allow the distinction between the two possible pictures. The situation changes however as regards the possibility of fast rotation of strange stars. This has its origin in the completely different mass-radius relations of neutron and strange stars (see Fig. 10) [59]. As a consequence of this the entire family of strange stars can rotate rapidly – i.e., considerably below one millisecond –, not just those near the limit of gravitational collapse to a black hole as is the case for neutron stars. Furthermore, as I shall discuss below, the cooling history of neutron stars and strange

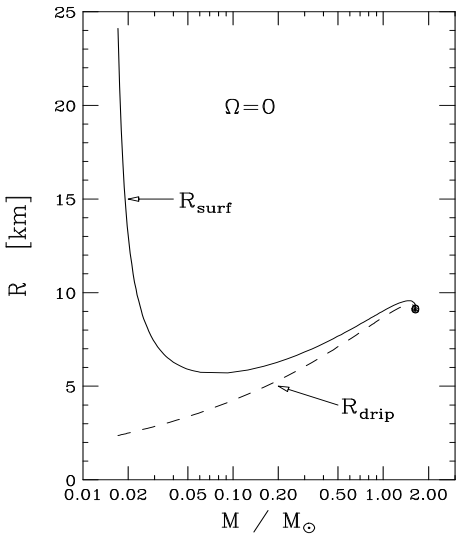

Figure 10: Radius as a function of mass of a non-rotating strange star with crust [89].

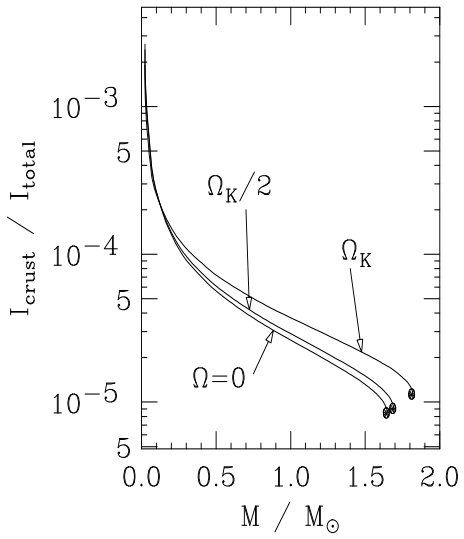

Figure 11: The ratio $I_{\rm crust}/I_{\rm total}$ as a function of star mass. Rotational frequencies are shown as a fraction of the Kepler frequency, $\Omega_{\rm K}$ [33].

stars may be quite different.

5.2 Hadronic crust on strange stars and pulsar glitches

At the present time there appears to be only one crucial astrophysical test of the strange-quark-matter hypothesis, and that is whether strange quark stars can give rise to the observed phenomena of pulsar glitches. In the crust quake model an oblate solid nuclear crust in its present shape slowly comes out of equilibrium with the forces acting on it as the rotational period changes, and fractures when the built up stress exceeds the sheer strength of the crust material. The period and rate of change of period slowly heal to the trend preceding the glitch as the coupling between crust and core re-establish their co-rotation. The existence of glitches may have a decisive impact on the question of whether strange matter is the ground state of the strong interaction.

The only existing investigation which deals with the calculation of the thickness, mass and moment of inertia of the nuclear solid crust that can exist on the surface of a rotating, general relativistic strange quark star has only recently been performed by Glendenning and Weber [89]. Their calculated mass-radius relationship for strange stars with a nuclear crust, whose maximum density is the neutron drip density, is shown in Fig. 10. (Free neutrons in the star cannot exist. These would be dissolved into quark matter as they gravitate into the strange core. Therefore the maximum density of the crust is strictly limited by neutron drip. This density is about 4.3×10^{11} g/cm^3.) Since the crust is bound by the gravitational interaction (and not

by confinement, which is the case for the strange matter core), the relationship is qualitatively similar to the one for neutron and hybrid stars, as can be seen from Fig. 6. The radius being largest for the lightest and smallest for the heaviest stars (indicated by the soid dot in Fig. 10) in the sequence. Just as for neutron stars the relationship is not necessarily monotonic at intermediate masses. The radius of the strange quark core, denoted $R_{\rm drip}$, is shown by the dashed line. (A value for the bag constant of $B^{1/4} = 160$ MeV for which 3-flavor strange matter is absolutely stable has been chosen. This choice represents weakly bound strange matter with an energy per baryon ~ 920 MeV, and thus corresponds to strange quark matter being absolutely bound with respect to ^{56}Fe). The radius of the strange quark core is proportional to $M^{1/3}$ which is typical for self-bound objects. This proportionality is only modified near that stellar mass where gravity terminates the stable sequence. The sequence of stars has a minimum mass of $\sim 0.015\,M_\odot$ (radius of ~ 400 km) or about 15 Jupiter masses, which is considerably smaller than that of neutron star sequences, about $0.1\ M_\odot$ [113]. The low-mass strange stars may be of considerable importance since they may be difficult to detect and therefore may effectively hide baryonic matter. Furthermore, of interest to the subject of cooling of strange stars is the crust thickness of strange stars [114]. It ranges from $\sim$ 400 km for stars at the lower mass limit to ~ 12 km for stars of mass $\sim 0.02\,M_\odot$, and is a fraction of a kilometer for the star at the maximum mass [89].

The moment of inertia of the hadronic crust, $I_{\rm crust}$, that can be carried by a strange star as a function of star mass for a sample of rotational frequencies of $\Omega = \Omega_{\rm K}, \Omega_{\rm K}/2$ and 0 is shown in Fig. 11. Because of the relatively small crust mass of the maximum-mass models of each sequence, the ratio $I_{\rm crust}/I_{\rm total}$ is smallest for them (solid dots in Fig. 11). The less massive the strange star the larger its radius (Fig. 10) and therefore the larger both $I_{\rm crust}$ as well as $I_{\rm total}$. The dependence of $I_{\rm crust}$ and $I_{\rm total}$ on M is such that their ratio $I_{\rm crust}/I_{\rm total}$ is a monotonically decreasing function of M. One sees that there is only a slight difference between $I_{\rm crust}$ for $\Omega = 0$ and $\Omega = \Omega_{\rm K}/2$.

Of considerable relevance for the question of whether strange stars can exhibit glitches in rotation frequency, one sees that $I_{\rm crust}/I_{\rm total}$ varies between 10^{-3} and $\sim 10^{-5}$ at the maximum mass. If the angular momentum of the pulsar is conserved in the quake then the relative frequency change and moment of inertia change are equal, and one arrives at [89]

$$\frac{\Delta\Omega}{\Omega} \;=\; \frac{|\Delta I|}{I_0} \;>\; \frac{|\Delta I|}{I} \;\equiv\; f\,\frac{I_{\rm crust}}{I} \;\sim\; (10^{-5} - 10^{-3})\,f\ , \ \text{with} \quad 0 < f < 1\ . \qquad (27)$$

Here I_0 denotes the moment of inertia of that part of the star whose frequency is changed in the quake. It might be that of the crust only, or some fraction, or all of the star. The factor f in Eq. (27) represents the fraction of the crustal moment of inertia that is altered in the quake, i.e., $f \equiv |\Delta I|/I_{\rm crust}$. Since the observed glitches have relative frequency changes $\Delta\Omega/\Omega = (10^{-9} - 10^{-6})$, a change in the crustal moment of inertia of $f \lesssim 0.1$ would cause a giant glitch even in the least favorable case (for more details, see [89]). Moreover, we find that the observed range of the fractional change in the spin-down rate, $\dot{\Omega}$, is consistent with the crust having the small moment of inertia calculated and the quake involving only a small fraction f of

that, just as in Eq. (27). For this purpose we write [89]

$$\frac{\Delta\dot{\Omega}}{\dot{\Omega}} \;=\; \frac{\Delta\dot{\Omega}/\dot{\Omega}}{\Delta\Omega/\Omega}\,\frac{|\Delta I|}{I_0} \;=\; \frac{\Delta\dot{\Omega}/\dot{\Omega}}{\Delta\Omega/\Omega}\,f\,\frac{I_{\rm crust}}{I_0} \;>\; (10^{-1}\ \text{to}\ 10)\,f\ , \tag{28}$$

where use of Eq. (27) has been made. Equation (28) yields a small f value, i.e., $f < (10^{-4}$ to $10^{-1})$, in agreement with $f \lesssim 10^{-1}$ established just above. Here measured values of the ratio $(\Delta\Omega/\Omega)/(\Delta\dot{\Omega}/\dot{\Omega}) \sim 10^{-6}$ to 10^{-4} for the Crab and Vela pulsars, respectively, have been used.

5.3 Thermal evolution of neutron and strange stars

The left panel of Fig. 12 shows a numerical simulation of the thermal evolution of neutron stars. The neutrino emission rates are determined by the modified and direct Urca processes, and the presence of a pion or kaon condensate. The baryons are treated as superfluid particles. Hence the neutrino emissivities are suppressed by an exponential factor of $\exp(-\Delta/kT)$, where Δ is the width of the superfluid gap (see Ref. [115] for details). Due to the dependence of the direct Urca process and the onset of meson condensation on star mass, stars that are too light for these processes to occur (i.e., $M < 1\,M_\odot$) are restricted to standard cooling via modified Urca. Enhanced cooling via the other three processes results in a sudden drop of the star's surface temperature after about 10 to 10^3 years after birth, depending on the thickness of the ionic crust. As one sees, agreement with the observed data is achieved only if different masses for the underlying pulsars are assumed. The right panel of Fig. 12 shows cooling simulations of strange quark stars. The curves differ with respect to assumptions made about a possible superfluid behavior of the quarks. Because of the higher neutrino emission rate in non-superfluid quark matter, such quark stars cool most rapidly (as long as cooling is core dominated). In this case one does not get agreement with most of the observed pulsar data. The only exception is pulsar PSR 1929+10. Superfluidity among the quarks reduces the neutrino emission rate, which delays cooling [115]. This moves the cooling curves into the region where most of the observed data lie.

Subject to the inherent uncertainties in the behavior of strange quark matter as well as superdense nuclear matter, at present it appears much too premature to draw any definitive conclusions about the true nature of observed pulsars. Nevertheless, should a continued future analysis in fact confirm a considerably faster cooling of strange stars relative to neutron stars, this would provide a definitive signature (together with rapid rotation) for the identification of a strange star. Specifically, the prompt drop in temperature at the very early stages of a pulsar, say within the first 10 to 50 years after its formation, could offer a good signature of strange stars [114]. This feature, provided it withstands a more rigorous analysis of the microscopic properties of quark matter, could become particularly interesting if continued observation of SN 1987A would reveal the temperature of the possibly existing pulsar at its center.

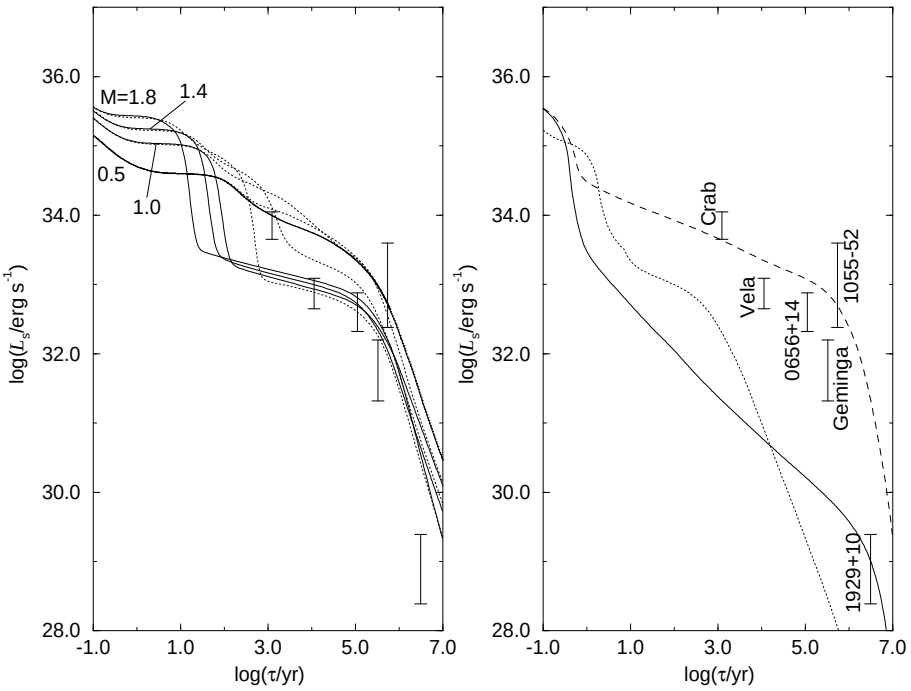

Figure 12: Left panel: Cooling of neutron stars with pion (solid curves) or kaon condensates (dotted curve). Right panel: Cooling of $M = 1.8\,M_\odot$ strange stars with crust. The cooling curves of lighter strange stars, e.g. $M \gtrsim 1\,M_\odot$, differ only insignificantly from those shown here. Three different assumptions about a possible superfluid behavior of strange quark matter are made: no superfluidity (solid), superfluidity of all three flavors (dotted), and superfluidity of up and down flavors only (dashed). The vertical bars denote luminosities of observed pulsars.

6 Summary

This work begins with an investigation of the properties of superdense neutron star matter. Various models for the associated equation of state of such matter are introduced and their characteristic features are discussed in great detail. These equations of state are then applied to the construction of models of non-rotating as well as rotating compact stars, and an investigation of their cooling behavior. The theoretically computed neutron star properties are compared with the body of observed data.

The indication of this work is that the gravitational radiation-reaction driven instability in neutron stars sets a lower limit on stable rotation for massive neutron stars of $P \approx 0.8$ ms. Lighter ones having typical pulsar masses of $1.45\,M_\odot$ are predicted to have stable rotational periods $P \gtrsim 1$ ms. This finding may have very important implications for the nature of any pulsar that is found to have a shorter period, say around $P \approx 0.5$ ms. Since our representative collection of nuclear equations of state does not allow for rotation at such small periods, the interpretation of such objects as rapidly rotating neutron stars would fail. Such objects, however, can be understood

as rapidly rotating strange stars. The plausible ground-state state in that event is the deconfined phase of (3-flavor) strange quark matter. From the QCD energy scale this is as likely a ground-state as the confined phase of atomic matter. At the present time there appears to be only one crucial astrophysical test of the strange quark matter hypothesis, and that is whether strange quark stars can give rise to the observed phenomena of pulsar glitches. We demonstrate that the nuclear solid crust that can exist on the surface of a strange star can have a moment of inertia sufficiently large that a fractional change can account for the magnitude of pulsar glitches. Furthermore low-mass strange stars can have enormously large nuclear crusts (up to several thousand kilometers [116, 117]) which enables such objects to be possible hiding places of baryonic matter. Finally, due to the uncertainties in the behavior of superdense nuclear as well as strange matter, we conclude that no definitive conclusions about the true nature (strange or conventional) of observed pulsars can be drawn from cooling simulations yet. As of yet, they could be made of strange quark matter as well as of conventional nuclear matter.

Acknowledgement: This work was supported by the Director, Office of Energy Research, Office of High Energy and Nuclear Physics, Division of Nuclear Physics, and of the U.S. Department of Energy under Contract DE-AC03-76SF00098.

References

[1] R. N. Manchester and J. H. Taylor, *Pulsars*, W. H. Freeman and Co., San Francisco, 1977.

[2] D. C. Backer, S. R. Kulkarni, C. Heiles, M. M. Davis, and W. M. Goss, Nature **300** (1982) 615.

[3] R. N. Manchester, A. G. Lyne, C. Robinson, N. D'Amico, M. Bailes, and J. Lim, Nature **352** (1991) 219.

[4] J. L. Friedman, J. R. Ipser, and L. Parker, Astrophys. J. **304** (1986) 115.

[5] J. L. Friedman, J. R. Ipser, and L. Parker, Phys. Rev. Lett. **62** (1989) 3015.

[6] J. M. Lattimer, M. Prakash, D. Masak, and A. Yahil, Astrophys. J. **355** (1990) 241.

[7] F. Weber, N. K. Glendenning, and M. K. Weigel, Astrophys. J. **373** (1991) 579.

[8] F. Weber and N. K. Glendenning, Astrophys. J. **390** (1992) 541.

[9] F. Weber and N. K. Glendenning, *Hadronic Matter and Rotating Relativistic Neutron Stars*, Proceedings of the Nankai Summer School, "Astrophysics and Neutrino Physics", p. 64–183, Tianjin, China, 17-27 June 1991, ed. by D. H. Feng, G. Z. He, and X. Q. Li, World Scientific, Singapore, 1993.

[10] E. Witten, Phys. Rev. D **30** (1984) 272.

[11] C. Alcock, E. Farhi, and A. V. Olinto, Astrophys. J. **310** (1986) 261.

[12] P. Haensel, J. L. Zdunik, and R. Schaeffer, Astron. Astrophys. **160** (1986) 121.

[13] D. W. L. Sprung, Adv. Nucl. Phys. **5** (1972) 225.

[14] B. D. Day, Rev. Mod. Phys. **51** (1979) 821.

[15] V. R. Pandharipande and R. B. Wiringa, Rev. Mod. Phys. **51** (1979) 821.

[16] R. B. Wiringa, V. Fiks, and A. Fabrocini, Phys. Rev. C **38** (1988) 1010.

[17] N. K. Glendenning, Astrophys. J. **293** (1985) 470.

[18] K. Holinde, K. Erkelenz, and R. Alzetta, Nucl. Phys. **A194** (1972) 161; **A198** (1972) 598.

[19] R. Machleidt, K. Holinde, and Ch. Elster, Phys. Rep. **149** (1987) 1.

[20] N. K. Glendenning, Phys. Lett. **114B** (1982) 392;
N. K. Glendenning, Astrophys. J. **293** (1985) 470;
N. K. Glendenning, Z. Phys. A **326** (1987) 57;
N. K. Glendenning, Z. Phys. A **327** (1987) 295.

[21] F. Weber and M. K. Weigel, Nucl. Phys. **A505** (1989) 779.

[22] P. C. Martin and J. Schwinger, Phys. Rev. **115** (1959) 1342.

[23] L. Wilets, Green's functions method for the relativistic field theory many-body problem, in *Mesons in nuclei*, Vol. III, ed. by M. Rho, D. Wilkinson, North-Holland, Amsterdam, 1979.

[24] H. Huber, F. Weber, and M. K. Weigel, Phys. Lett. **317B** (1993) 485.

[25] H. Huber, F. Weber, and M. K. Weigel, Phys. Rev. C **50** (1994) R1287.

[26] H. Huber, F. Weber, and M. K. Weigel, Phys. Rev. C **51** (1995) 1790.

[27] P. Poschenrieder and M. K. Weigel, Phys. Lett. **200B** (1988) 231;
P. Poschenrieder and M. K. Weigel, Phys. Rev. C **38** (1988) 471.

[28] F. Weber and M. K. Weigel, Z. Phys. A**330** (1988) 249.

[29] F. Weber and M. K. Weigel, J. Phys. G **15** (1989) 765.

[30] B. D. Serot and J. D. Walecka, Adv. Nucl. Phys. **16** (1986) 1.

[31] C. J. Horowitz and B. D. Serot, Nucl. Phys. **A464** (1987) 613.

[32] N. K. Glendenning, Nucl. Phys. **A493** (1989) 521.

[33] N. K. Glendenning, Nucl. Phys. B (Proc. Suppl.) **24B** (1991) 110.

[34] N. K. Glendenning, Phys. Rev. D **46** (1992) 1274.

[35] N. K. Glendenning, F. Weber, and S. A. Moszkowski, Phys. Rev. C **45** (1992) 844.

[36] N. K. Glendenning, Phys. Rev. Lett. **57** (1986) 1120.

[37] H. A. Bethe and M. Johnson, Nucl. Phys. **A230** (1974) 1.

[38] B. Friedman and V. R. Pandharipande, Nucl. Phys. **A361** (1981) 502.

[39] W. D. Myers and W. J. Swiatecki, Ann. Phys. (N. Y.) **204** (1990) 401.

[40] W. D. Myers and W. J. Swiatecki, Ann. Phys. (N. Y.) **211** (1991) 292.

[41] W. D. Myers and W. J. Swiatecki, "The Nuclear Thomas-Fermi Model", presented by W. J. Swiatecki at the XXIX Zakopane School of Physics, September 5–14, 1994, Zakopane, Poland, (LBL-36004).

[42] W. D. Myers and W. J. Swiatecki, "Thomas Fermi Treatment of Nuclear Masses, Deformations and Density Distributions", presented by W. J. Swiatecki at the Fourth KINR International School on Nuclear Physics, Kiev, Russia, August 29–September 7, 1994, Zakopane, Poland, (LBL-36005).

[43] V. R. Pandharipande, Nucl. Phys. **A178** (1971) 123.

[44] V. R. Pandharipande and R. B. Wiringa, Nucl. Phys. **A449** (1986) 219.

[45] R. B. Wiringa, R.A. Smith, and T. L. Ainsworth, Phys. Rev. C **29** (1984) 1207.

[46] I. E. Lagaris and V. R. Pandharipande, Nucl. Phys. **A359** (1981) 349.

[47] W. D. Myers, *Droplet Model of Atomic Nuclei* (New York: McGraw Hill, 1977);
W. D. Myers and W. Swiatecki, Ann. of Phys. **55** (1969) 395;
W. D. Myers and K.-H. Schmidt, Nucl. Phys. **A410** (1983) 61.

[48] P. K. Banerjee and D. W. L. Sprung, Can. J. Phys. **49** (1971) 1871.

[49] C. Mahaux, *Brueckner Theory of Infinite Fermi Systems*, Lecture Notes in Physics, Vol. 138, (Springer Verlag, Berlin, 1981).

[50] E. O. Fiset and T. C. Foster, Nucl. Phys. **A184** (1972) 588.

[51] Q. Ho-Kim and F. C. Khanna, Ann. Phys. **86** (1974) 233.

[52] F. Weber and M. K. Weigel, Phys. Rev. C **32** (1985) 2141.

[53] F. Coester, S. Cohen, B. Day, and C. M. Vincent, Phys. Rev. C **1** (1970) 769.

[54] C. W. Wong, Ann. Phys. (N. Y.) **72** (1972) 107.

[55] L. S. Celenza and C. M. Shakin, Phys. Rev. C **24** (1981) 2704.

[56] L. S. Celenza and C. M. Shakin, *Relativistic Nuclear Structure Physics*, World Scientific Lecture Notes in Physics, Vol. 2, World Scientific, Singapore, 1986.

[57] B. ter Haar and R. Malfliet, Phys. Rev. Lett. **59** (1987) 1652.

[58] F. Weber and N. K. Glendenning, Phys. Lett. **265B** (1991) 1.

[59] N. K. Glendenning, *Supernovae, Compact Stars and Nuclear Physics*, invited paper in Proc. of 1989 Int. Nucl. Phys. Conf., Sao Paulo, Brasil, Vol. 2, ed. by M. S. Hussein et al., World Scientific, Singapore, 1990.

[60] N. K. Glendenning, *Strange-Quark-Matter Stars*, Proc. Int. Workshop on Relativ. Aspects of Nucl. Phys., Rio de Janeiro, Brasil, 1989, ed. by T. Kodama, K. C. Chung, S. J. B. Duarte, and M. C. Nemes, World Scientific, Singapore, 1990.

[61] J. Ellis, J. I. Kapusta, and K. A. Olive, Nucl. Phys. **B348** (1991) 345.

[62] G. Baym and S. Chin, Phys. Lett. **62B** (1976) 241.

[63] B. D. Keister and L. S. Kisslinger, Phys. Lett. **64B** (1976) 117.

[64] G. Chapline and M. Nauenberg, Phys. Rev. D **16** (1977) 450.

[65] W. B. Fechner and P. C. Joss, Nature **274** (1978) 347.

[66] H. A. Bethe, G. E. Brown, and J. Cooperstein, Nucl. Phys. **A462** (1987) 791.

[67] B. D. Serot and H. Uechi, Ann. Phys. (N. Y.) **179** (1987) 272.

[68] W. D. Arnett and R. L. Bowers, Astrophys. J. Suppl. **33** (1977) 415.

[69] J. H. Taylor and J. M. Weisberg, Astrophys. J. **345** (1989) 434.

[70] S. E. Thorsett, Z. Arzoumanian, M. M. McKinnon, and J. H. Taylor, Astrophys. J. **405** (1993) L29.

[71] S. A. Rappaport and P. C. Joss, *Accrection Driven Stellar X-Ray Sources*, ed. by W. H. G. Lewin and E. P. J. van den Heuvel, Cambridge University Press, 1983.

[72] F. Nagase, Publ. Astron. Soc. Japan **41** (1989) 1.

[73] N. K. Glendenning, *Nuclear and Particle Astrophysics*, Proc. Int. Summer School on the Structure of Hadrons and Hadronic Matter, Dronten, Netherlands, August 5-18, 1990, ed. by O. Scholten and J. H. Koch, World Scientific, Singapore, 1991, p. 275.

[74] J. Van Paradijs, Astrophys. J. **234** (1978) 609.

[75] S. L. Shapiro and S. A. Teukolsky, *Black Holes, White Dwarfs, and Neutron Stars*, John Wiley & sons, N. Y., 1983.

[76] M. Y. Fujimoto and R. E. Taam, Astrophys. J. **305** (1986) 246.

[77] M. Ruderman, Ann. Rev. Astr. Ap. **10** (1972) 427.

[78] G. Baym and C. Pethick, Ann. Rev. Nucl. Sci. **25** (1975) 27.

[79] V. Trimble and M. Rees, Astrophys. Lett. **5** (1970) 93.

[80] G. Borner and J. M. Cohen, Astrophys. J. **185** (1973) 959.

[81] E. P. Liang, Astrophys. J. **304** (1986) 682.

[82] K. Brecher and A. Burrows, Astrophys. J. **240** (1980) 642.

[83] R. Ramaty and P. Meszaros, Astrophys. J. **250** (1981) 384.

[84] J. R. Oppenheimer and G. M. Volkoff, Phys. Rev. **55** (1939) 374.

[85] Ch. W. Misner, K. S. Thorne, and J. A. Wheeler, *Gravitation*, W. H. Freeman and Company, San Francisco, 1973.

[86] R. Ruffini, in *Physics and Astrophysics of Neutron Stars and Black Holes* (North Holland, Amsterdam, 1978) p. 287.

[87] G. E. Brown and H. A. Bethe, Astrophys. J. **423** (1994) 659.

[88] H. A. Bethe and G. E. Brown, Astrophys. J. **445** (1995) L129.

[89] N. K. Glendenning and F. Weber, Astrophys. J. **400** (1992) 647.

[90] L. Lindblom, Astrophys. J. **303** (1986) 146.

[91] L. Lindblom, *Instabilities in Rotating Neutron Stars*, in The Structure and Evolution of Neutron Stars, Proceedings, ed. by D. Pines, R. Tamagaki, and S. Tsuruta, Addison-Wesley, 1992.

[92] F. Weber and N. K. Glendenning, Z. Phys. **A339** (1991) 211.

[93] S. Chandrasekhar, Phys. Rev. Lett. **24** (1970) 611.

[94] J. L. Friedman, Phys. Rev. Lett. **51** (1983) 11.

[95] L. Lindblom and S. L. Detweiler, Astrophys. J. **211** (1977) 565.

[96] S. L. Detweiler, Astrophys. J. **197** (1975) 203.

[97] H. Lamb, Proc. London Math. Soc. **13** (1881) 51.

[98] C. Cutler and L. Lindblom, Astrophys. J. **314** (1987) 234.

[99] J. R. Ipser and L Lindbolm, Phys. Rev. Lett. **62** (1989) 2777.

[100] J. R. Ipser and L. Lindblom, Astrophys. J. **355** (1990) 226.

[101] R. A. Managan, Astrophys. J. **309** (1986) 598.

[102] R. F. Sawyer, Phys. Rev. D **39** (1989) 3804.

[103] J. R. Ipser and L. Lindblom, Astrophys. J. **373** (1991) 213.

[104] F. Weber and N. K. Glendenning, *Impact of the Nuclear Equation of State on Models of Rotating Neutron Stars*, Proc. of the Int. Workshop on Unstable Nuclei in Astrophysics, Tokyo, Japan, June 7-8, 1991, ed. by S. Kubono and T. Kajino, World Scientific, Singapore, 1992, p. 307.

[105] N. K. Glendenning, Phys. Rev. D **46** (1992) 4161.

[106] N. K. Glendenning and F. Weber, Phys. Rev. D **50** (1994) 3836.

[107] N. K. Glendenning, Mod. Phys. Lett. **A5** (1990) 2197.

[108] F. Weber and N. K. Glendenning, *Interpretation of Rapidly Rotating Pulsars*, Proceedings of the Second International Symposium on Nuclear Astrophysics, "Nuclei in the Cosmos", Karlsruhe, Germany, July 6–10, 1992, ed. by F. Käppeler and K. Wisshak, IOP Publishing Ltd, Bristol, UK, 1993, p. 399.

[109] A. R. Bodmer, Phys. Rev. D **4** (1971) 1601.

[110] H. Terazawa, INS-Report-338 (INS, Univ. of Tokyo, 1979); J. Phys. Soc. Japan, **58** (1989) 3555; **58** (1989) 4388; **59** (1990) 1199.

[111] J. Madsen and M. L. Olesen, Phys. Rev. D **43** (1991) 1069, ibid., **44**, 566 (erratum).

[112] R. R. Caldwell and J. L. Friedman, Phys. Lett. **264B** (1991) 143.

[113] G. Baym, C. Pethick, and P. Sutherland, Astrophys. J. **170** (1971) 299.

[114] P. Pizzochero, Phys. Rev. Lett. **66** (1991) 2425.

[115] Ch. Schaab, F. Weber, M. K. Weigel, and N. K. Glendenning, Nucl. Phys. **A605** (1996) 531.

[116] N. K. Glendenning, Ch. Kettner, and F. Weber, Astrophys. J. **450** (1995) 253.

[117] N. K. Glendenning, Ch. Kettner, and F. Weber, Phys. Rev. Lett. **74** (1995) 3519.